ACS APPLIED NANO MATERIALS

www.acsanm.org Article

Exploring Maleimide-Based Nanoparticle Surface Engineering to Control Cellular Interactions

Joanne C. Lee,[#] Nathan D. Donahue,[#] Angelina S. Mao, Amber Karim, Mallikharjuna Komarneni, Emily E. Thomas, Emmy R. Francek, Wen Yang, and Stefan Wilhelm*

Cite This: https://dx.doi.org/10.1021/acsanm.9b02541 Read Online

ACCESS | Metrics & More | Article Recommendations | Supporting Information

ABSTRACT: Nanoparticle cellular interactions are governed by nanoparticle surface chemistry and the surface display of functional (bio)molecules. To conjugate and display thiol-containing (bio)-molecules on nanoparticle surfaces, reactions between thiols and functional maleimide groups are often exploited. However, current procedures for modifying nanoparticle surfaces with maleimide groups are complex and can result in nanoparticle aggregation. Here, we demonstrate a straightforward, fast (~30 min), efficient, and robust one-step surface engineering protocol for modifying gold nanoparticles with functional maleimide groups. We designed a hetero-bifunctional poly(ethylene glycol)-based molecule that attaches efficiently to the gold nanoparticle surface in a single step via its orthopyridyl disulfide (OPSS) terminal end, leaving its maleimide functional group available for downstream reaction with thiols. Using this surface engineering approach, we fabricated gold nanoparticles with near neutral and positive surface charges, respectively. We demonstrate that nanoparticle cellular uptake efficiencies in model mouse breast cancer (4T1) cells, human breast cancer (MDA-MB-231) cells, and human umbilical vein endothelial (HUVEC) cells in tissue culture can be tuned by up to 3 orders of magnitude by adjusting nanoparticle surface chemistry. Our straightforward and efficient maleimide-based nanoparticle surface engineering protocol creates a platform technology for controlled covalent surface attachment of a variety of thiol-containing (bio)molecules to nanoparticles for rational design of nanomaterials with precise cellular interactions for widespread applications in bioanalysis and nanomedicine.

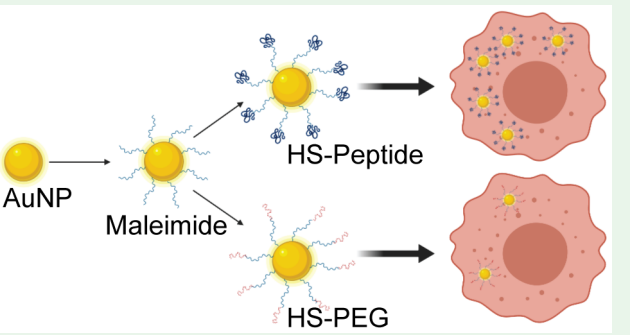

KEYWORDS: *nanoparticle, nanomedicine, maleimide−thiol chemistry, elemental analysis, OPSS PEG, breast cancer, surface modification*

INTRODUCTION

Nanoparticle physicochemical properties, including size, shape, and surface chemistry, are key factors in driving interactions between nanomaterials and biological systems, such as organs, tissues, and cells.[1−4] Interactions between these biological systems and engineered nanoparticles can be precisely tuned via rationally designed display of functional (bio)molecules on nanoparticle surfaces.[5] To modify surfaces of nanoparticles with (bio)molecules, such as nucleic acids, proteins, carbohydrates, and synthetic molecules like poly(ethylene glycol) (PEG), a number of different chemical conjugation strategies have been developed.[6−9] These strategies include carbodiimide chemistry, reactions with *N*-hydroxysuccinimide (NHS) active esters, and click chemistry reactions (e.g., azide−alkyne cycloadditions).[10−12]

Maleimide−thiol reactions are another important and widely used strategy to covalently join maleimide functional groups with sulfhydryls.[13,14] This chemistry favors mild reaction conditions at near neutral pH and can be performed in aqueous media at room temperature with high conjugation efficiency. In addition, maleimides exhibit high chemical selectivity toward thiol functional groups.[15] These advantages make maleimide−thiol chemistry an attractive strategy for the covalent conjugation of (bio)molecules to nanoparticle surfaces to form succinimidyl thioethers, which exhibit good long-term stability in physiological environments.[16]

A number of organic and inorganic nanomaterials have been described in the literature to exploit maleimide−thiol chemistry for surface functionalization and covalent attachment of (bio)molecules and drugs.[17−19] However, most current methods of maleimide surface functionalization are complex multistep procedures and time-consuming. For example, one common protocol involves functionalization of furan-protected maleimide−PEG−thiols to gold nanoparticles and subsequent generation of maleimide groups via retro-Diels−Alder reactions that require heating at 95 °C for 2 h and

Received: December 19, 2019
Accepted: February 10, 2020
Published: February 10, 2020

https://dx.doi.org/10.1021/acsanm.9b02541
ACS Appl. Nano Mater. XXXX, XXX, XXX−XXX

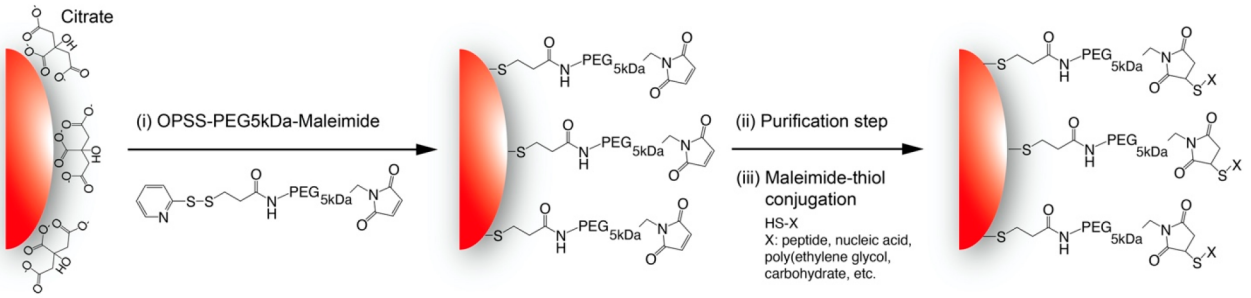

Figure 1. Schematic representation of maleimide-based nanoparticle surface functionalization. (i) OPSS-(PEG)5kDa-Mal is conjugated to the surface of citrate-stabilized gold nanoparticles (depicted by red surface) via a ligand exchange reaction to form maleimide-functionalized nanoparticles. (ii) Maleimide-functionalized nanoparticles are then purified by centrifugation to remove excess OPSS-(PEG)5kDa-Mal. (iii) Virtually any molecule with accessible thiol groups can then be conjugated to the nanoparticles via maleimide−thiol chemistry.

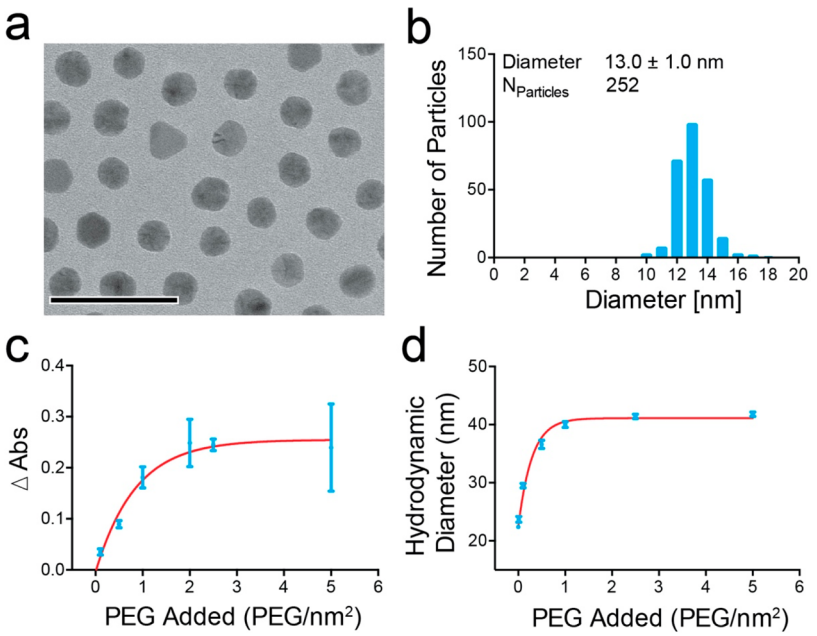

Figure 2. Synthesis, characterization, and surface modification of 13 nm AuNPs. (a) Transmission electron micrograph (TEM) of 13 nm AuNPs. Scale bar indicates 50 nm. (b) Nanoparticle size distribution histogram based on image analysis of TEM micrographs. (c) UV−vis spectrophotometry-based OPSS-(PEG)5kDa-Mal depletion assay to quantify the maximum nanoparticle surface loading capacity. Absorbance was measured at 283 nm. The starting absorbance (Abs_0) of OPSS-(PEG)5kDa-Mal was subtracted by the absorbance of OPSS-(PEG)5kDa-Mal in the supernatant (Abs_{SN}) after incubating AuNPs with different amounts of OPSS-(PEG)5kDa-Mal (PEG added per nm^2 of nanoparticle surface area) to give ΔAbs. It is assumed that ΔAbs corresponds to the amount of OPSS-(PEG)5kDa-Mal conjugated to the nanoparticle surface. The smooth curve is a guide to the eye. (d) To corroborate results from panel c, the hydrodynamic diameters of AuNPs incubated with different amounts of OPSS-(PEG)5kDa-Mal (PEG added per nm^2 of nanoparticle surface area) were measured. When the nanoparticle surface is saturated with PEG molecules, the hydrodynamic diameter stays constant, indicating a saturation brush conformation of conjugated PEG ligands. The smooth curve is a guide to the eye. PEG surface densities used for these experiments were 0, 0.01, 0.1, 0.5, 1, 2.5, and 5 OPSS-(PEG)5kDa-Mal per nm^2 of nanoparticle surface area. Mean values ± standard deviation (n = 3).

the use of organic solvents.[20−22] Another common procedure uses an exchange reaction with cetyltrimethylammonium bromide (CTAB) functionalized nanoparticles and HS−PEG−amine with a subsequent reaction of the amine groups with 4-(*N*-maleimidomethyl)cyclohexane-1-carboxylic acid 3-sulfo-*N*-hydroxysuccinimide ester sodium salt (sulfo-SMCC) carrying a maleimide group at the opposite terminal end.[23] These laborious procedures exhibit multiple chemical reaction steps and are challenging to control. Recently, a different and more user-friendly approach was reported that involves a thioctic acid functionalized PEG molecule terminated with a maleimide group.[24] The thioctic acid can conjugate to the gold nanoparticle through disulfide bonds. However, this procedure requires an overnight incubation step and titration to pH 10−11, which could potentially result in substantial hydrolysis of maleimide groups.[25] Other protocols for modifying nanoparticle surfaces with maleimide groups report the use of retro-Michael-type addition and functionalizing the gold nanoparticles with azide-terminated PEG to then use copper-free click chemistry for the attachment of maleimide groups.[26,27] In summary, nanoparticle surface modification protocols to display maleimide functional groups are time-consuming and complex and may result in irreversible nanoparticle aggregation.

Here, we explore a fast and simple single step maleimide functionalization method to engineer the surface of gold nanoparticles. Our method is robust, is easy to use, and requires only ∼30 min to execute. We used a rationally

https://dx.doi.org/10.1021/acsanm.9b02541
ACS Appl. Nano Mater. XXXX, XXX, XXX−XXX

designed hetero-bifunctional orthopyridyl disulfide (OPSS)-based PEG molecule with a terminal maleimide group. The OPSS terminal end is attached to the gold nanoparticle surface via the gold−sulfur interaction, while the maleimide group is free to react with virtually any molecule with an accessible sulfhydryl functional group. The reaction can be conducted at room temperature under physiological pH with high yield. Our surface engineering strategy is broadly applicable to a range of gold nanoparticle diameters from 4 to 100 nm and can be used in conjunction with PEG backfilling strategies to minimize nonspecific interactions with proteins and other (bio)-molecules.[28] We demonstrate that by use of this straightforward and robust protocol, the surface of gold nanoparticles can be precisely designed to control nanoparticle interactions with model mouse breast cancer (4T1) cells, human breast cancer cells (MDA-MB-231), and human umbilical vein endothelial cells (HUVEC) in cell culture.

RESULTS AND DISCUSSION

Our general procedure for modifying gold nanoparticle surfaces with maleimide groups is shown in Figure 1. To attach and display maleimide functional groups on the surface of gold nanoparticles, citrate-stabilized nanoparticles are mixed with a rationally designed hetero-bifunctional orthopyridyl disulfide (OPSS)-based PEG molecule with a terminal maleimide group. This OPSS-based PEG derivative was designed in-house and custom-made by Laysan Bio, Inc. Following a ligand exchange reaction for ∼30 min at room temperature, the weakly bound citrate surface ligands are replaced by OPSS-(PEG)5kDa-Mal, resulting in modification of the gold nanoparticle surface with maleimide groups.[29] These surface-displayed maleimide groups are highly functional and can then react in a subsequent step with virtually any (bio)molecules that exhibit accessible thiol groups via a robust and established maleimide−thiol reaction.[30] The result of this reaction is the covalent attachment of a variety of different (bio)molecules to the gold nanoparticle surface (Figure 1).

To study the surface modification of gold nanoparticles with OPSS-(PEG)5kDa-Mal, we used 13 nm citrate-stabilized gold nanoparticles as model nanoparticles, since these nanoparticles can be synthesized reproducibly with high yield.[11] Transmission electron microscopy (TEM)-based characterization studies shown in Figures 2a and 2b confirm that these nanoparticles exhibit narrow (≤10%) size distributions with uniform shape.

Using these monodisperse 13 nm citrate-stabilized gold nanoparticles, we then tested our surface engineering method by quantifying the maximum surface conjugation capacity of OPSS-(PEG)5kDa-Mal molecules. We titrated a fixed amount of 13 nm gold nanoparticles with increasing amounts of OPSS-(PEG)5kDa-Mal and determined the surface binding capacity using two independent analytical techniques: (i) UV−vis spectrophotometry (Figure 2c) and (ii) dynamic light scattering (DLS, Figure 2d). On the basis of these titration studies, we determined the PEG surface saturation points, i.e., the maximum number of OPSS-(PEG)5kDa-Mal per nm^2 of nanoparticle surface area. Using absorbance measurements at 283 nm (Figures S1−S3), we determined the amount of OPSS-(PEG)5kDa-Mal in solution before (Abs_0) and after conjugation (Abs_{SN}) of gold nanoparticles to calculate ΔAbs. The ΔAbs value is a quantitative measure for the maximum loading capacity of OPSS-(PEG)5kDa-Mal onto the gold nanoparticle surfaces (Figure 2c). The point at which ΔAbs remains constant can be considered as the maximum PEG surface density where there is no more room available for additional OPSS-(PEG)5kDa-Mal to bind to the nanoparticle surface. As direct evidence for the presence of OPSS-(PEG)5kDa-Mal groups on the surface of gold nanoparticles and for the successful surface modification of gold nanoparticles with OPSS-(PEG)5kDa-Mal, we performed X-ray photoelectron spectroscopy (XPS) analysis. In agreement with previous literature reports, our XPS analysis results confirm that OPSS groups bind via thiolates to gold nanoparticle surfaces (peak at 162.18 eV; Figure S11) rather than disulfides; i.e., the disulfide bond is cleaved upon surface conjugation.[29] As a second line of direct evidence for the presence of OPSS-(PEG)5kDa-Mal groups on the surface of gold nanoparticles, we performed ^{1}H NMR studies (Figure S12). Collectively, our XPS and ^{1}H NMR studies confirm the successful conjugation of OPSS-(PEG)5kDa-Mal to gold nanoparticles.

To corroborate the PEGylation saturation curve obtained by UV−vis spectrophotometry (Figure 2c), we probed the hydrodynamic diameter of gold nanoparticles incubated with different amounts of OPSS-(PEG)5kDa-Mal per nm^2 of nanoparticle surface area. By use of dynamic light scattering (DLS), the increase in hydrodynamic diameter of nanoparticles incubated with increasing amounts of OPSS-(PEG)-5kDa-Mal per nm^2 of nanoparticle surface area indicated the successful attachment of OPSS-(PEG)5kDa-Mal molecules to gold nanoparticle surfaces. Based on literature reports, this increase could potentially be explained by a change in PEG ligand conformation. At low PEG surface density, the predominant PEG conformation is the mushroom conformation, while a higher PEG surface density (>1 PEG/nm^2) indicates a more fully extended brush layer conformation.[31,32] In line with our UV−vis spectrophotometry-based results (Figure 2c), DLS experiments corroborated that the maximum conjugation capacity of OPSS-(PEG)5kDa-Mal is between 1 and 2 OPSS-(PEG)5kDa-Mal per nm^2 for 13 nm gold nanoparticles (Table S3). The results are further supported by qualitative agarose gel electrophoresis experiments of 13 nm gold nanoparticles titrated with increasing amounts of OPSS-(PEG)5kDa-Mal per nm^2 (Figure S4). In summary, these data suggest that (i) the nanoparticle surface modification with OPSS-(PEG)5kDa-Mal was successful and (ii) the theoretical number of maleimide groups per nanoparticle surface unit area available for downstream conjugation of thiol-containing (bio)molecules is between 1 and 2 maleimide/nm^2. If we assume an OPSS-(PEG)5kDa-Mal surface saturation density of ∼1.5 PEG/nm^2 (Table S3), we can estimate the number of maleimide groups per 13 nm gold nanoparticle to be ∼800. It is worth noting that our nanoparticle surface engineering method is robust, straightforward, and efficient and only requires mixing of an OPSS-(PEG)5kDa-Mal aqueous solution with an aqueous gold nanoparticle dispersion and subsequent incubation at room temperature for 30 min. This makes our procedure faster (minutes vs multiple hours) and more efficient (minimal hydrolysis of maleimide groups within 30 min) than previous methods.[23,20,24]

Next, to determine how the observed surface saturation behavior of OPSS-(PEG)5kDa-Mal varies with nanoparticle size, we titrated a range of different gold nanoparticles from 4 to 100 nm with increasing amounts of PEG. Transmission electron microscopy and image analysis of corresponding micrographs reveal the narrow size distribution and uniform

https://dx.doi.org/10.1021/acsanm.9b02541
ACS Appl. Nano Mater. XXXX, XXX, XXX−XXX

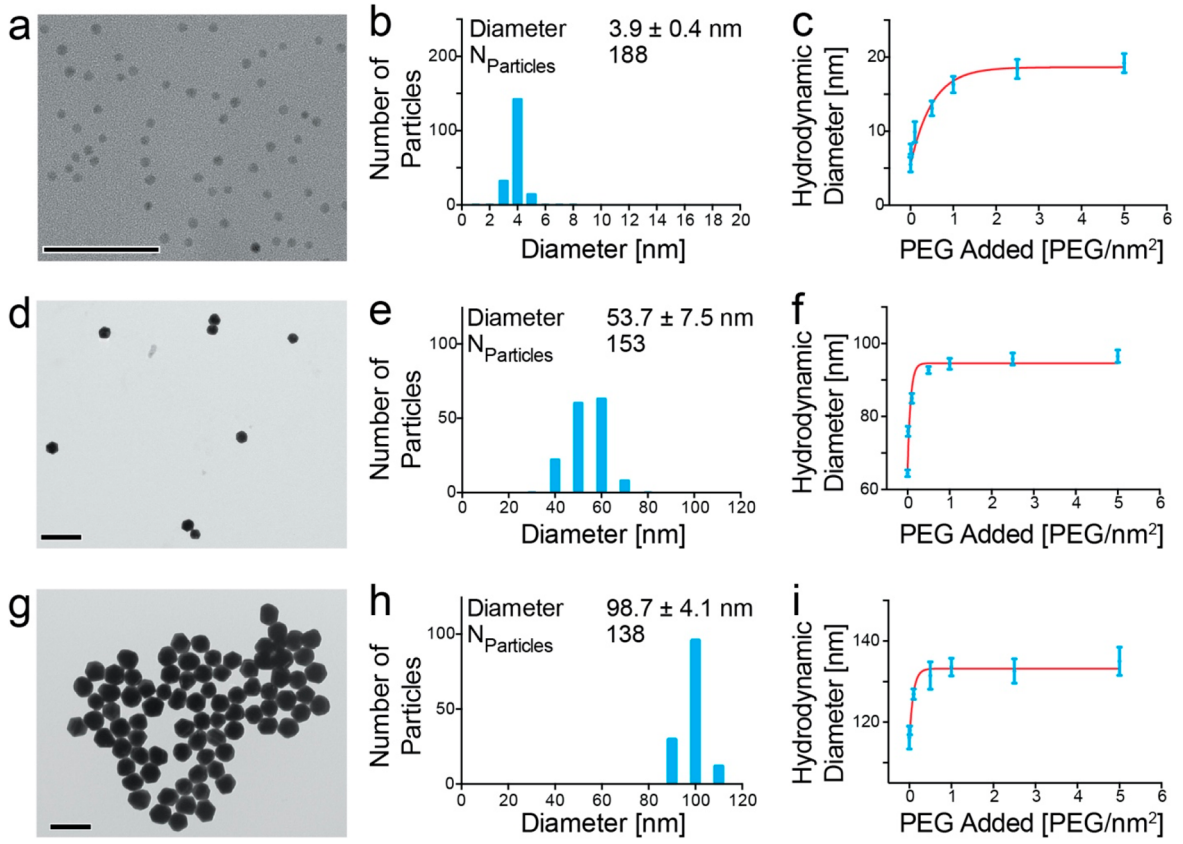

Figure 3. Synthesis, characterization, and surface modification of 4, 50, and 100 nm gold nanoparticles. Panels a–c display data for 4 nm gold nanoparticles (AuNPs). (a) TEM micrograph of 4 nm AuNPs. Scale bars represent 50 nm. (b) Nanoparticle size distribution histogram based on image analysis of TEM micrographs. (c) Hydrodynamic diameter of as a function of OPSS-(PEG)5kDa-Mal added to AuNPs per nm^2 of nanoparticle surface area. The smooth curve is a guide to the eye. Panels d–f display data for 50 nm AuNPs. (d) TEM micrograph of 50 nm AuNPs. Scale bars represent 200 nm. (e) Nanoparticle size distribution histogram based on image analysis of TEM micrographs. (f) Hydrodynamic diameter of as a function of OPSS-(PEG)5kDa-Mal added to AuNPs per nm^2 of nanoparticle surface area. The smooth curve is a guide to the eye. Panels g–i display data for 100 nm AuNPs. (g) TEM micrograph of 100 nm AuNPs. Scale bars represent 200 nm. (h) Nanoparticle size distribution histogram based on image analysis of TEM micrographs. (i) Hydrodynamic diameter as a function of OPSS-(PEG)5kDa-Mal added to AuNPs per nm^2 of nanoparticle surface area. The smooth curve is a guide to the eye. Amount of PEG for panels corresponds to 0, 0.01, 0.1, 0.5, 1, 2.5, and 5 OPSS-(PEG)5kDa-Mal per nm^2 of nanoparticle surface area. Mean values ± standard deviation (n = 3).

shape of gold nanoparticles (Figure 3). To explore the PEG nanoparticle surface loading capacity, we titrated nanoparticles with increasing amounts of OPSS-(PEG)5kDa-Mal per nm^2 of nanoparticle surface area and quantified corresponding hydrodynamic diameters using DLS (Figure 3c,f,i). We observed that larger nanoparticles (i.e., 50 and 100 nm gold nanoparticles) exhibit saturation characteristics at lower PEG surface densities compared to 4 and 14 nm gold nanoparticles (Table S3). This finding indicates that nanoparticle curvature may play a role in saturation of PEG surface ligand binding.[33] For example, 4 nm gold nanoparticles undergo saturation at ∼3 PEG/nm^2 while 50 and 100 nm undergo saturation at PEG surface densities below 1 PEG/nm^2 (Figure 3 and Table S3). To further confirm our results obtained with DLS analysis, we characterized the electrophoretic migration of differently sized gold nanoparticles with varying PEG surface densities using agarose gel electrophoresis. As shown in Figure S4, the electrophoretic migration of larger, more neutral, and surface saturated gold nanoparticles is restricted by the pore size of the agarose gel while smaller, more negative, and unsaturated nanoparticles move more easily through the agarose gel. These findings corroborate the saturation characteristics of the different gold nanoparticle sizes seen by using DLS analysis (Figure 3 and Figure S4). Taken together, our data confirm that our surface engineering procedure using OPSS-(PEG)-5kDa-Mal can be successfully applied to a broad range of gold nanoparticle sizes. Depending on the nanoparticle size, the maximum amount of OPSS-(PEG)5kDa-Mal that can be conjugated per nm^2 of nanoparticles surface is controlled by nanoparticle surface curvature.

To determine whether nanoparticles modified with OPSS-(PEG)5kDa-Mal could chemically bind thiol-containing (bio)-molecules, we tested four different ligands: (i) a short cationic peptide composed of polylysine with a terminal cysteine moiety termed here as K_7C (KKKKKKKC), (ii) a thiol-containing 5 kDa PEG chain terminated with a methoxy group (thiol-PEG5kDa-OCH_3), (iii) a thiol-containing 1-kDa PEG chain terminated with a methoxy group (thiol-(PEG)1kDa-OCH_3), and (iv) a thiol-containing PEG chain terminated with an amine group (thiol-(PEG)5kDa-NH_2) (Figure S5).

As shown in Figure 4a, the hydrodynamic diameter of 13 nm citrate-stabilized gold nanoparticles increased by ∼16 nm upon conjugation of 2 OPSS-(PEG)5kDa-Mal per nm^2 of nanoparticle surface area. In a subsequent conjugation step, the maleimide groups then reacted with thiol-containing (bio)-molecules to further increase the nanoparticle hydrodynamic

https://dx.doi.org/10.1021/acsanm.9b02541
ACS Appl. Nano Mater. XXXX, XXX, XXX−XXX

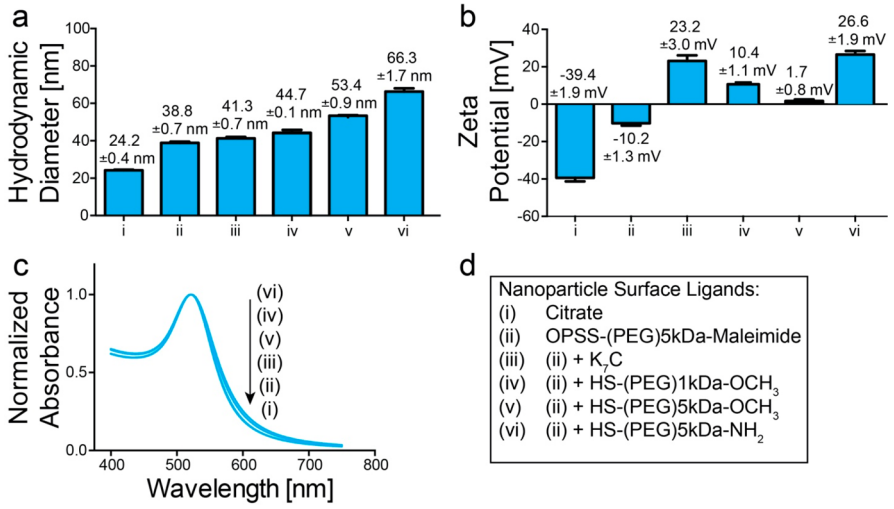

Figure 4. Nanoparticle surface conjugation of four different ligands using maleimide−thiol chemistry. (a) Hydrodynamic diameter measurements of 13 nm gold nanoparticles functionalized with (i) citrate ligands, (ii) OPSS-(PEG)5kDa-Mal, (iii) OPSS-(PEG)5kDa-Mal and K_7C, (iv) OPSS-(PEG)5kDa-Mal and HS-(PEG)5kDa-OCH_3, (v) OPSS-(PEG)5kDa-Mal and HS-(PEG)1kDa-OCH_3, and (vi) OPSS-(PEG)5kDa-Mal and HS-(PEG)5kDa-NH_2. Mean values ± standard deviation (n = 3). (b) ζ-potential measurements of the gold nanoparticles functionalized with different surface ligands. Mean values ± standard deviation (n = 3). (c) Normalized UV−vis absorption spectra of 13 nm gold nanoparticles conjugated to different surface ligands. (d) Legend of gold nanoparticle surface modifications for each data plot.

diameter. Interestingly, as the molecular weight of ligands increased from K_7C to HS-(PEG)1kDa-methoxy, HS-(PEG)-5kDa-methoxy, and HS-(PEG)5kDa-amine, the overall hydrodynamic diameter of nanoparticles also increased, indicating successful ligand conjugation. Successful surface conjugation of different thiol-containing ligands was further confirmed by ζ-potential measurements. By use of citrate-coated and maleimide-modified gold nanoparticles as control groups, these ζ-potential measurements reveal a significant shift to near neutral or positive mV values that reflect the expected neutral or cationic charge characteristics of corresponding ligands at neutral pH (Figure 4b). While we observed an increase of the nanoparticle hydrodynamic diameter and change in nanoparticle ζ-potential in a ligand-dependent manner, the polydispersity indices (PDI) for all nanoparticle conjugates remained below 0.1, indicating that nanoparticles remained monodisperse and colloidally stable after surface modification (Figure S6). These results are further corroborated by consistent UV−vis absorption spectra for all nanoparticle conjugates (Figure 4c). Proton NMR studies provide further direct evidence for the successful covalent conjugation of thiol-containing ligands to functional maleimide groups on the nanoparticle surface (Figure S13). Collectively, we confirmed the successful surface conjugation of different thiol-containing ligands (Figure 4d) to maleimide-modified gold nanoparticles with four independent analytical techniques: (i) DLS, (ii) ζ-potential analysis, (iii) UV−vis spectrophotometry, and (iv) 1H NMR. Our results indicate that (i) our maleimide-based surface modification protocol is broadly applicable to a wide range of different gold nanoparticle sizes and (ii) maleimide surface groups are available for subsequent covalent conjugation with a variety of different thiol-containing (bio)molecular ligands.

In 2014, Dai et al. demonstrated that active targeting of ligand-conjugated nanoparticles to corresponding cellular receptors overexpressed on cancer cell surfaces is affected by the nanoparticle protein corona.[28] To minimize the negative effect of the nanoparticle protein corona on ligand−receptor interactions used for active targeting in nanomedicine, Dai and colleagues developed a method that is termed nanoparticle surface PEG backfilling. Briefly, targeting ligands, such as monoclonal antibodies, are covalently conjugated to longer PEG chains on the nanoparticle surface, while the remaining nanoparticle surface is backfilled with shorter PEG chains to minimize nonspecific adsorption of serum proteins. To qualitatively demonstrate that our maleimide-based surface engineering protocol is compatible with such a PEG backfilling strategy, we systematically compared colloidal stability of three different surface modified gold nanoparticles under high salt concentrations (i.e., ∼0.45 M sodium chloride). As shown in Figure S6, dispersions of citrate-coated gold nanoparticles and gold nanoparticles modified with 0.01 OPSS-(PEG)5kDa-MAL/nm^2 aggregate under high salt concentrations, indicated by the blue/purple color of the corresponding aqueous dispersions. In contrast, dispersions of 13 nm gold nanoparticles modified with 0.01 OPSS-(PEG)5kDa-MAL/nm^2 and backfilled with 5 OPSS-(PEG)2kDa-OCH_3/nm^2 retain their ruby red color, indicating colloidal stability even under high salt concentrations. It is important to note that we intentionally used a PEG derivative with a disulfide group for backfilling (i.e., OPSS-(PEG)2kDa-OCH_3) rather than a thiol-terminated PEG derivative to prevent reactions between PEG and nanoparticle surface-bound maleimide groups. This approach leaves the surface-bound maleimide groups intact and available for subsequent reactions with thiol-containing (bio)molecules (Table S2). In summary, our results suggest that (i) our maleimide-based surface engineering procedure is compatible with PEG backfilling strategies and (ii) PEG-backfilled nanoparticles exhibit improved colloidal stability in comparison to non-backfilled nanoparticles (Figure S6). Additional colloidal stability tests indicate that OPSS-based gold nanoparticle surface modifications exhibit similar performance as commonly used thiol-based ligand attachments to gold nanoparticle surfaces (Table S5).

Finally, we explored the feasibility of our maleimide-based surface engineering strategy to control interactions between

https://dx.doi.org/10.1021/acsanm.9b02541
ACS Appl. Nano Mater. XXXX, XXX, XXX−XXX

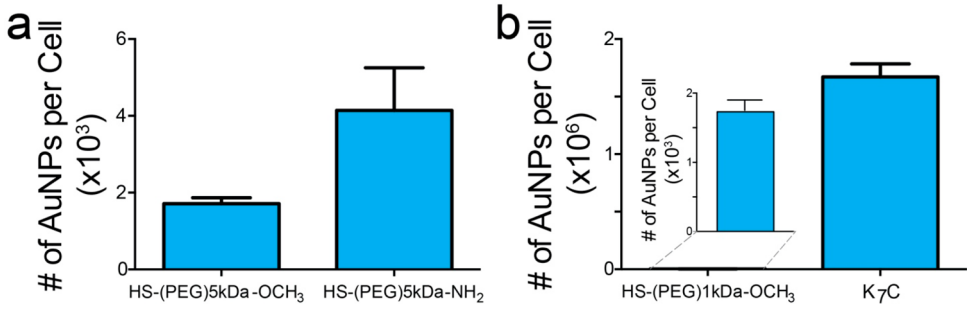

Figure 5. Uptake of OPSS-(PEG)5kDa-MAL-modified 13 nm gold nanoparticles (AuNPs) functionalized with different neutral and cationic ligands in 4T1 mouse breast cancer cells in tissue culture. (a) Cell uptake of AuNPs conjugated to HS-(PEG)5kDa-OCH_3 vs cell uptake of AuNPs functionalized with HS-(PEG)5kDa-NH_2. Amine-terminated PEG increases AuNPs cell uptake by a factor of 2 compared to methoxy-terminated PEG. (b) Cell uptake of AuNPs conjugated to HS-(PEG)1kDa-OCH_3 vs AuNPs functionalized with K_7C peptide. The K_7C peptide increases AuNPs cell uptake by 3 orders of magnitude compared to methoxy-terminated PEG (see the inset). Mean values ± standard deviation (n = 4).

nanoparticles and cells. By exposing model mouse breast cancer cells (4T1) to different types of surface-modified 13 nm gold nanoparticles in tissue culture, we quantified the cellular uptake using inductively coupled plasma mass spectrometry (ICP-MS) analysis. The ICP-MS elemental analysis technique allows precise quantification of gold content within acid-digested cells samples to estimate the average number of gold nanoparticles per cell. As shown in Figure 5, we compared 4T1 cellular uptake of four different nanoparticle types. All four types of nanoparticles were produced by using our maleimide-based surface engineering strategy. In short, 13 nm citrate-coated nanoparticles were modified with 2 OPSS-(PEG)5kDa-Mal/nm^2 first, followed by backfilling with 5 OPSS-(PEG)-2kDa-OCH_3 to minimize any nonspecific interactions. Next, one of four model thiol-containing ligands was conjugated via maleimide−thiol chemistry: (i) HS-(PEG)5kDa-NH_2, (ii) HS-(PEG)5kDa-OCH_3, (iii) K_7C, and (iv) HS-(PEG)1kDa-OCH_3. DLS confirmed successful conjugation and colloidal stability in cell culture media (Table S2.

To explore the effect of nanoparticle surface charge on cellular uptake, we performed two different comparisons. In the first comparison, we chose HS-(PEG)5kDa-OCH_3 as an overall neutral PEG derivative ligand and HS-(PEG)5kDa-NH_2 as a positively charged PEG ligand to create nanoparticles with overall neutral and cationic ζ-potential (Figure 4b). As shown in Figure 5a, cellular uptake increased by a factor of ∼2 for cationic nanoparticles in comparison to more neutral HS-(PEG)5kDa-OCH_3 surface-modified nanoparticles. To determine the effect of cationic peptide ligands on nanoparticle cell uptake, we conjugated K_7C onto maleimide-coated gold nanoparticles (Figure 4b). This group of nanoparticles was compared to an overall neutral HS-(PEG)1kDa-OCH_3 ligand with similar molecular weight as K_7C, i.e., ∼1 kDa. As determined by quantitative ICP-MS analysis, the cellular uptake of K_7C-modified nanoparticles increased by ∼3 orders of magnitude compared to nanoparticles modified with HS-(PEG)1kDa-OCH_3 (Figure 5b). As K_7C peptides consist of seven protonated lysine residues at near neutral pH, they bear a substantial positive ζ-potential in a similar range as the HS-(PEG)5kDa-NH_2-modified nanoparticles (∼25 mV). These results indicate that nanoparticles with overall positive ζ-potential exhibit higher cell uptake efficiencies than their more neutral counterparts. Current reports suggest that since cell membranes bear an overall negative charge, the Coulombic interactions between the cationic nanoparticles and the negatively charged membrane may lead to increased cellular uptake.[34−37] When comparing HS-(PEG)5kDa-NH_2-modified nanoparticles to K_7C peptide-modified nanoparticles, an increase in nanoparticle cellular uptake of ∼3 orders of magnitude is observed (Figure 5). These data suggest that besides the ζ-potential there are other parameters that drive nanoparticle cellular uptake. For example, polylysine-based nanoconjugates have been reported to enhance cellular uptake due to strong overall positive ζ-potential and amphipathic activity.[38,39] In this study, the exact biomolecular mechanisms of how nanoparticles interact with cells have not been studied in detail. We plan on investigating these mechanisms in more detail in future studies.

To demonstrate that our nanoparticle surface engineering approach is compatible with different types of cells, we incubated human umbilical vein endothelial cells (HUVECs) and human breast cancer (MDA-MB-231) cells with surface modified nanoparticles. As shown in Figure S8, K_7C peptide-modified nanoparticles increased cellular uptake in HUVECs by ∼26 times compared to PEGylated nanoparticles. Transmission electron micrographs of human breast cancer MDA-MB-231 confirm that nanoparticles are taken up into intracellular vesicles (Figure S9). Results from the viability assay on 4T1 cancer cells demonstrated decreases in viability for nanoparticles modified with cationic surfaces but no effect on cell viability for nanoparticle designs with neutral surface charges (Figure S10). It has been reported that nanoparticles bearing cationic surface modifications can induce cell membrane disruption, organelle damage, and cell necrosis.[40−43]

In summary, our maleimide-based surface engineering strategy allows precise control over nanoparticle−cell interactions by engineering nanoparticle physicochemical and biological properties to enhance cellular uptake.

■ CONCLUSIONS

We have developed a straightforward, fast (∼30 min), and robust one-step surface engineering protocol for modifying gold nanoparticles with functional maleimide groups. In our approach, we used a hetero-bifunctional PEG-based molecule termed OPSS-(PEG)5kDa-MAL. This molecule can be attached to gold nanoparticles in a single step via its orthopyridyl disulfide (OPSS) terminal end, leaving its maleimide functional group available for downstream reaction with thiols. The chemoselectivity of the maleimide−thiol chemistry enables virtually any ligand (bio)molecule with free thiols to preferentially react and bind to the terminal

https://dx.doi.org/10.1021/acsanm.9b02541
ACS Appl. Nano Mater. XXXX, XXX, XXX−XXX

maleimide groups displayed on gold nanoparticles at room temperature and physiological pH. In addition, the chemoselectivity of this reaction can increase regioselectivity to ensure that biomolecules preferentially conjugate with their thiol terminal end to nanoparticles for site-specific molecular attachment.

We have demonstrated that the surface density of maleimide groups can be controlled for a variety of different gold nanoparticle sizes. Considering the effects of how chemical regioselectivity of biomolecular ligands and ligand spacing on the nanoparticle surface impact cellular interactions and ligand receptor binding, our approach may be particularly useful for applications involving attachment of biomolecules to nanoparticle surfaces.[44,45] In principle, our nanoparticle surface engineering approach will allow conjugation of a wide range of thiol-containing biomolecules, including cell-penetrating peptides, biosensing oligonucleotides, and targeting antibodies for diverse applications in nanomedicine and biosensing.[46−50] Using this surface engineering approach, we fabricated gold nanoparticles with near neutral and positive surface charges that exhibited surface charge dependent cellular uptake efficiencies in different model cell lines in tissue culture. Our maleimide-based nanoparticle surface engineering protocol is a platform technology that permits controlled covalent attachment of a variety of thiol-containing (bio)molecules to enable rational designing of nanomaterials with precise cellular interactions for applications in bioanalysis and nanomedicine.

■ ASSOCIATED CONTENT

Supporting Information

The Supporting Information is available free of charge at https://pubs.acs.org/doi/10.1021/acsanm.9b02541.

Detailed descriptions of materials and methods used for nanoparticle synthesis, surface modifications, and characterization; Figures S1−S13 and Tables S1−S5 (PDF)

■ AUTHOR INFORMATION

Corresponding Author

Stefan Wilhelm − *Stephenson School of Biomedical Engineering, University of Oklahoma, Norman, Oklahoma 73019, United States; Stephenson Cancer Center, Oklahoma City, Oklahoma 73104, United States; Institute for Biomedical Engineering, Science, and Technology (IBEST), Norman, Oklahoma 73019, United States;* orcid.org/0000-0003-2167-6221; Email: stefan.wilhelm@ou.edu

Authors

Joanne C. Lee − *Stephenson School of Biomedical Engineering, University of Oklahoma, Norman, Oklahoma 73019, United States*

Nathan D. Donahue − *Stephenson School of Biomedical Engineering, University of Oklahoma, Norman, Oklahoma 73019, United States*

Angelina S. Mao − *Norman North High School, Norman, Oklahoma 73069, United States*

Amber Karim − *Stephenson School of Biomedical Engineering, University of Oklahoma, Norman, Oklahoma 73019, United States*

Mallikharjuna Komarneni − *School of Chemical, Biological, and Materials Engineering, University of Oklahoma, Norman, Oklahoma 73019, United States*

Emily E. Thomas − *Stephenson School of Biomedical Engineering, University of Oklahoma, Norman, Oklahoma 73019, United States*

Emmy R. Francek − *Stephenson School of Biomedical Engineering, University of Oklahoma, Norman, Oklahoma 73019, United States*

Wen Yang − *Stephenson School of Biomedical Engineering, University of Oklahoma, Norman, Oklahoma 73019, United States*

Complete contact information is available at: https://pubs.acs.org/10.1021/acsanm.9b02541

Author Contributions

#J.C.L. and N.D.D. contributed equally to this paper.

Author Contributions

J.C.L. and S.W. designed the study. All authors contributed to experiments and analyzed the data. J.C.L., N.D.D., and S.W. wrote the manuscript. All authors contributed to manuscript editing. We also thank Biorender for their technical support.

Notes

The authors declare no competing financial interest.

■ ACKNOWLEDGMENTS

The authors thank Dr. Larson for help with electron microscopy, Dr. Foster for support with ICP-MS, and Dr. Harrison for the 4T1 cells. The authors acknowledge experimental assistance from Ms. Lee, Ms. Schwemley, Ms. Woodward, Ms. Karim, and Mr. Donaldson. J.C.L. thanks the Office of Undergraduate Research and the Honors Research Assistant Program for funding. S.W. acknowledges funding from the University of Oklahoma Junior Faculty Fellowship (JFF) and University of Oklahoma IBEST-OUHSC Funding for Interdisciplinary Research Seed Grant.

■ REFERENCES

(1) Donahue, N. D.; Acar, H.; Wilhelm, S. Concepts of Nanoparticle Cellular Uptake, Intracellular Trafficking, and Kinetics in Nanomedicine. *Adv. Drug Delivery Rev.* **2019**, *143*, 68−96.

(2) Albanese, A.; Tang, P. S.; Chan, W. C. W. The Effect of Nanoparticle Size, Shape, and Surface Chemistry on Biological Systems. *Annu. Rev. Biomed. Eng.* **2012**, *14* (1), 1−16.

(3) Narum, S. M.; Le, T.; Le, D. P.; Lee, J. C.; Donahue, N. D.; Yang, W.; Wilhelm, S. Passive Targeting in Nanomedicine: Fundamental Concepts, Body Interactions, and Clinical Potential. In *Nanoparticles for Biomedical Applications*; Elsevier: 2020; pp 37−53.

(4) Huai, Y.; Hossen, M. N.; Wilhelm, S.; Bhattacharya, R.; Mukherjee, P. Nanoparticle Interactions with the Tumor Microenvironment. *Bioconjugate Chem.* **2019**, *30* (9), 2247−2263.

(5) Conde, J.; Dias, J. T.; Grazú, V.; Moros, M.; Baptista, P. V.; de la Fuente, J. M. Revisiting 30 Years of Biofunctionalization and Surface Chemistry of Inorganic Nanoparticles for Nanomedicine. *Front. Chem.* **2014**, *2*, 48.

(6) Hermanson, G. T. *Bioconjugate Techniques*; Elsevier: 2008.

(7) Muhr, V.; Wilhelm, S.; Hirsch, T.; Wolfbeis, O. S. Upconversion Nanoparticles: From Hydrophobic to Hydrophilic Surfaces. *Acc. Chem. Res.* **2014**, *47* (12), 3481−3493.

(8) Wilhelm, S.; Hirsch, T.; Patterson, W. M.; Scheucher, E.; Mayr, T.; Wolfbeis, O. S. Multicolor Upconversion Nanoparticles for Protein Conjugation. *Theranostics* **2013**, *3* (4), 239−248.

(9) Wilhelm, S.; Kaiser, M.; Würth, C.; Heiland, J.; Carrillo-Carrion, C.; Muhr, V.; Wolfbeis, O. S.; Parak, W. J.; Resch-Genger, U.; Hirsch, T. Water Dispersible Upconverting Nanoparticles: Effects of Surface Modification on Their Luminescence and Colloidal Stability. *Nanoscale* **2015**, *7* (4), 1403−1410.

(10) Lin, C.-A. J.; Sperling, R. A.; Li, J. K.; Yang, T.-Y.; Li, P.-Y.; Zanella, M.; Chang, W. H.; Parak, W. J. Design of an Amphiphilic Polymer for Nanoparticle Coating and Functionalization. *Small* **2008**, *4* (3), 334−341.
(11) Dai, Q.; Wilhelm, S.; Ding, D.; Syed, A. M.; Sindhwani, S.; Zhang, Y.; Chen, Y. Y.; MacMillan, P.; Chan, W. C. W. Quantifying the Ligand-Coated Nanoparticle Delivery to Cancer Cells in Solid Tumors. *ACS Nano* **2018**, *12* (8), 8423−8435.
(12) Zhu, K.; Zhang, Y.; He, S.; Chen, W.; Shen, J.; Wang, Z.; Jiang, X. Quantification of Proteins by Functionalized Gold Nanoparticles Using Click Chemistry. *Anal. Chem.* **2012**, *84* (10), 4267−4270.
(13) Ghosh, S. S.; Kao, P. M.; McCue, A. W.; Chappelle, H. L. Use of Maleimide-Thiol Coupling Chemistry for Efficient Syntheses of Oligonucleotide-Enzyme Conjugate Hybridization Probes. *Bioconjugate Chem.* **1990**, *1* (1), 71−76.
(14) Gindy, M. E.; Ji, S.; Hoye, T. R.; Panagiotopoulos, A. Z.; Prud'homme, R. K. Preparation of Poly(Ethylene Glycol) Protected Nanoparticles with Variable Bioconjugate Ligand Density. *Biomacromolecules* **2008**, *9* (10), 2705−2711.
(15) Martínez-Jothar, L.; Doulkeridou, S.; Schiffelers, R. M.; Sastre Torano, J.; Oliveira, S.; van Nostrum, C. F.; Hennink, W. E. Insights into Maleimide-Thiol Conjugation Chemistry: Conditions for Efficient Surface Functionalization of Nanoparticles for Receptor Targeting. *J. Controlled Release* **2018**, *282*, 101−109.
(16) Fontaine, S. D.; Reid, R.; Robinson, L.; Ashley, G. W.; Santi, D. V. Long-Term Stabilization of Maleimide-Thiol Conjugates. *Bioconjugate Chem.* **2015**, *26* (1), 145−152.
(17) Gobbo, P.; Biesinger, M. C.; Workentin, M. S. Facile Synthesis of Gold Nanoparticle (AuNP)-Carbon Nanotube (CNT) Hybrids through an Interfacial Michael Addition Reaction. *Chem. Commun.* **2013**, *49* (27), 2831−2833.
(18) Hwu, J. R.; Lin, Y. S.; Josephrajan, T.; Hsu, M.-H.; Cheng, F.-Y.; Yeh, C.-S.; Su, W.-C.; Shieh, D.-B. Targeted Paclitaxel by Conjugation to Iron Oxide and Gold Nanoparticles. *J. Am. Chem. Soc.* **2009**, *131*, 66−68.
(19) Ravi, S.; Krishnamurthy, V. R.; Caves, J. M.; Haller, C. A.; Chaikof, E. L. Maleimide-Thiol Coupling of a Bioactive Peptide to an Elastin-like Protein Polymer. *Acta Biomater.* **2012**, *8* (2), 627−635.
(20) Zhu, J.; Waengler, C.; Lennox, R. B.; Schirrmacher, R. Preparation of Water-Soluble Maleimide-Functionalized 3 nm Gold Nanoparticles: A New Bioconjugation Template. *Langmuir* **2012**, *28* (13), 5508−5512.
(21) Gobbo, P.; Workentin, M. S. Improved Methodology for the Preparation of Water-Soluble Maleimide-Functionalized Small Gold Nanoparticles. *Langmuir* **2012**, *28* (33), 12357−12363.
(22) Zhu, J.; Chin, J.; Wängler, C.; Wängler, B.; Lennox, R. B.; Schirrmacher, R. Rapid 18F-Labeling and Loading of PEGylated Gold Nanoparticles for in Vivo Applications. *Bioconjugate Chem.* **2014**, *25* (6), 1143−1150.
(23) Ba, H.; Rodríguez-Fernández, J.; Stefani, F. D.; Feldmann, J. Immobilization of Gold Nanoparticles on Living Cell Membranes upon Controlled Lipid Binding. *Nano Lett.* **2010**, *10* (8), 3006−3012.
(24) Oh, E.; Susumu, K.; Blanco-Canosa, J. B.; Medintz, I. L.; Dawson, P. E.; Mattoussi, H. Preparation of Stable Maleimide-Functionalized Au Nanoparticles and Their Use in Counting Surface Ligands. *Small* **2010**, *6* (12), 1273−1278.
(25) Dixit, V.; Van Den Bossche, J.; Sherman, D. M.; Thompson, D. H.; Andres, R. P. Synthesis and Grafting of Thioctic Acid-PEG-Folate Conjugates onto Au Nanoparticles for Selective Targeting of Folate Receptor-Positive Tumor Cells. *Bioconjugate Chem.* **2006**, *17* (3), 603−609.
(26) Weissman, M. R.; Winger, K. T.; Ghiassian, S.; Gobbo, P.; Workentin, M. S. Insights on the Application of the Retro Michael-Type Addition on Maleimide-Functionalized Gold Nanoparticles in Biology and Nanomedicine. *Bioconjugate Chem.* **2016**, *27* (3), 586−593.
(27) Nieves, D. J.; Azmi, N. S.; Xu, R.; Lévy, R.; Yates, E. A.; Fernig, D. G. Monovalent Maleimide Functionalization of Gold Nanoparticles via Copper-Free Click Chemistry. *Chem. Commun.* **2014**, *50* (86), 13157−13160.
(28) Dai, Q.; Walkey, C.; Chan, W. C. W. Polyethylene Glycol Backfilling Mitigates the Negative Impact of the Protein Corona on Nanoparticle Cell Targeting. *Angew. Chem., Int. Ed.* **2014**, *53* (20), 5093−5096.
(29) Lu, H. B.; Campbell, C. T.; Castner, D. G. Attachment of Functionalized Poly(Ethylene Glycol) Films to Gold Surfaces. *Langmuir* **2000**, *16* (4), 1711−1718.
(30) Northrop, B. H.; Frayne, S. H.; Choudhary, U. Thiol-Maleimide "Click" Chemistry: Evaluating the Influence of Solvent, Initiator, and Thiol on the Reaction Mechanism, Kinetics, and Selectivity. *Polym. Chem.* **2015**, *6* (18), 3415−3430.
(31) Cruje, C.; Chithrani, D. B. Polyethylene Glycol Functionalized Nanoparticles for Improved Cancer Treatment. *Rev. Nanosci. Nanotechnol.* **2014**, *3* (1), 20−30.
(32) Sperling, R. A.; Parak, W. J. Surface Modification, Functionalization and Bioconjugation of Colloidal Inorganic Nanoparticles. *Philos. Trans. R. Soc., A* **2010**, *368* (1915), 1333−1383.
(33) Lin, J.; Zhang, H.; Morovati, V.; Dargazany, R. PEGylation on Mixed Monolayer Gold Nanoparticles: Effect of Grafting Density, Chain Length, and Surface Curvature. *J. Colloid Interface Sci.* **2017**, *504*, 325−333.
(34) Ayala, V.; Herrera, A. P.; Latorre-Esteves, M.; Torres-Lugo, M.; Rinaldi, C. Effect of Surface Charge on the Colloidal Stability and in Vitro Uptake of Carboxymethyl Dextran-Coated Iron Oxide Nanoparticles. *J. Nanopart. Res.* **2013**, *15* (8), 1874.
(35) Jiang, Y.; Huo, S.; Mizuhara, T.; Das, R.; Lee, Y.-W.; Hou, S.; Moyano, D. F.; Duncan, B.; Liang, X.-J.; Rotello, V. M. The Interplay of Size and Surface Functionality on the Cellular Uptake of Sub-10 Nm Gold Nanoparticles. *ACS Nano* **2015**, *9* (10), 9986−9993.
(36) Wang, C.; Sun, A.; Qiao, Y.; Zhang, P.; Ma, L.; Su, M. Cationic Surface Modification of Gold Nanoparticles for Enhanced Cellular Uptake and X-Ray Radiation Therapy. *J. Mater. Chem. B* **2015**, *3* (37), 7372−7376.
(37) Vigderman, L.; Manna, P.; Zubarev, E. R. Quantitative Replacement of Cetyl Trimethylammonium Bromide by Cationic Thiol Ligands on the Surface of Gold Nanorods and Their Extremely Large Uptake by Cancer Cells. *Angew. Chem., Int. Ed.* **2012**, *51* (3), 636−641.
(38) Zorko, M.; Langel, Ü. Cell-Penetrating Peptides: Mechanism and Kinetics of Cargo Delivery. *Adv. Drug Delivery Rev.* **2005**, *57*, 529−545.
(39) Zhou, X.; Klibanov, A. L.; Huang, L. Lipophilic Polylysines Mediate Efficient DNA Transfection in Mammalian Cells. *Biochim. Biophys. Acta, Biomembr.* **1991**, *1065* (1), 8−14.
(40) Fröhlich, E. The Role of Surface Charge in Cellular Uptake and Cytotoxicity of Medical Nanoparticles. *Int. J. Nanomed.* **2012**, 5577−5591.
(41) Wei, X.; Shao, B.; He, Z.; Ye, T.; Luo, M.; Sang, Y.; Liang, X.; Wang, W.; Luo, S.; Yang, S.; et al. Cationic Nanocarriers Induce Cell Necrosis through Impairment of Na+/K+-ATPase and Cause Subsequent Inflammatory Response. *Cell Res.* **2015**, *25* (2), 237−253.
(42) Anguissola, S.; Garry, D.; Salvati, A.; O'Brien, P. J.; Dawson, K. A. High Content Analysis Provides Mechanistic Insights on the Pathways of Toxicity Induced by Amine-Modified Polystyrene Nanoparticles. *PLoS One* **2014**, *9* (9), No. e108025.
(43) Arvizo, R. R.; Miranda, O. R.; Thompson, M. A.; Pabelick, C. M.; Bhattacharya, R.; Robertson, J. D.; Rotello, V. M.; Prakash, Y. S.; Mukherjee, P. Effect of Nanoparticle Surface Charge at the Plasma Membrane and Beyond. *Nano Lett.* **2010**, *10* (7), 2543−2548.
(44) Schmid, D.; Park, C. G.; Hartl, C. A.; Subedi, N.; Cartwright, A. N.; Puerto, R. B.; Zheng, Y.; Maiarana, J.; Freeman, G. J.; Wucherpfennig, K. W. T Cell-Targeting Nanoparticles Focus Delivery of Immunotherapy to Improve Antitumor Immunity. *Nat. Commun.* **2017**, DOI: 10.1038/s41467-017-01830-8.
(45) Yang, Y.-S. S.; Moynihan, K. D.; Bekdemir, A.; Dichwalkar, T. M.; Noh, M. M.; Watson, N.; Melo, M.; Ingram, J.; Suh, H.; Ploegh, H.; et al. Targeting Small Molecule Drugs to T Cells with Antibody-

https://dx.doi.org/10.1021/acsanm.9b02541
ACS Appl. Nano Mater. XXXX, XXX, XXX−XXX

Directed Cell-Penetrating Gold Nanoparticles. *Biomater. Sci.* **2019**, *7* (1), 113−124.
(46) Wilhelm, S. Perspectives for Upconverting Nanoparticles. *ACS Nano* **2017**, *11* (11), 10644−10653.
(47) Sindhwani, S.; Syed, A. M.; Ngai, J.; Kingston, B. R.; Maiorino, L.; Rothschild, J.; MacMillan, P.; Zhang, Y.; Rajesh, N. U.; Hoang, T.; et al. The Entry of Nanoparticles into Solid Tumours. *Nat. Mater.* **2020**, 1−10.
(48) Syed, A. M.; MacMillan, P.; Ngai, J.; Wilhelm, S.; Sindhwani, S.; Kingston, B. R.; Wu, J. L. Y.; Llano-Suárez, P.; Lin, Z. P.; Ouyang, B. Liposome Imaging in Optically Cleared Tissues. *Nano Lett.* **2020**, DOI: 10.1021/acs.nanolett.9b04853.
(49) Poon, W.; Zhang, Y. N.; Ouyang, B.; Kingston, B.R.; Wu, J. L.; Wilhelm, S.; Chan, W. C. Elimination pathways of nanoparticles. *ACS Nano* **2019**, *13* (5), 5785−5798.
(50) Lazarovits, J.; Chen, Y. Y.; Song, F.; Ngo, W.; Tavares, A. J.; Zhang, Y.-N.; Audet, J.; et al. Synthesis of patient-specific nanomaterials. *Nano Lett.* **2019**, *19* (1), 116−123.

https://dx.doi.org/10.1021/acsanm.9b02541
ACS Appl. Nano Mater. XXXX, XXX, XXX−XXX